THE JOURNAL OF BIOLOGICAL CHEMISTRY
Vol. 278, No. 45, Issue of November 7, pp. 44921–44928, 2003
Printed in U.S.A.


# Compound Exocytosis and Cumulative Fusion in Eosinophils*

Received for publication, June 9, 2003, and in revised form, August 14, 2003
Published, JBC Papers in Press, August 15, 2003, DOI 10.1074/jbc.M306013200

**Ismail Hafez, Andreas Stolpe, and Manfred Lindau‡**

*From the School of Applied and Engineering Physics, Cornell University, Ithaca, New York 14853*

**Focal release of cytotoxic proteins by eosinophils onto the target surface plays an important role in parasite killing. Degranulation was stimulated by intracellular application of calcium and guanosine 5′-3-*O*-(thio)triphosphate via the recording patch pipette or via streptolysin-O permeabilization. Exocytotic fusion was monitored by capacitance measurements, whereas release of fluorescent weak bases, which accumulate selectively within eosinophil granules, was followed by fluorescence imaging. Several distinct types of granule fusion events were directly observed by simultaneous capacitance and fluorescence measurements. These are fusion of a single granule with the plasma membrane, intracellular granule-granule fusion, fusion of large compounds of pre-fused granules with the plasma membrane (compound exocytosis), and sequential fusion of granules to granules previously fused to the plasma membrane. Extensive granule-granule fusion was also observed by electron microscopy of permeabilized cells. All these fusion mechanisms contribute to focal release. The coexistence of distinct modes of exocytosis suggests that their regulation may modulate effector functions of eosinophils during helminth infection and allergic response.**

Eosinophils are involved in host defense against multicellular parasites (1) and have also been implicated in allergic asthmatic response (2). Parasite killing is mediated by adherence of eosinophils to the parasite surface followed by directed release of cytotoxic granule contents by exocytosis (3–5). Degranulation in eosinophils occurs through formation of degranulation sacs, which ensures release of cytotoxic proteins in high concentration at focal sites through a single fusion pore (3, 6). It is widely assumed that in eosinophils and basophils homotypic granule-granule fusion inside the cell leads to formation of compound granules followed by compound exocytosis, *i.e.* fusion of the compound with plasma membrane (6–9). Patch clamp capacitance measurements on horse eosinophils have suggested that in addition to compound exocytosis a mechanism of cumulative fusion exists, also leading to formation of a degranulation sac and focal release. Cumulative granule fusion is proposed to occur by fusion of a first granule with the plasma membrane followed by fusion of further granules with the already fused granule directing release of all granular contents through the initially formed fusion pore in the plasma membrane (5, 10).

Horse eosinophils contain particularly large granules (11) with a mean diameter of ≈1.5 μm, making them suitable for fluorescence imaging of single granule fusion events and patch clamp admittance analysis (5). By using electron microscopy and fluorescence imaging combined with square wave membrane capacitance measurements (5, 12, 13), we provide direct evidence of both mechanisms, compound exocytosis and cumulative fusion. In the accompanying paper (32) we show that the three different fusion processes, granule-granule fusion, granule-plasma membrane fusion, and granule-fused granule fusion, are differentially regulated.

## EXPERIMENTAL PROCEDURES

*Cell Preparation*—Eosinophils were isolated from 50–150 ml of fresh blood obtained from the jugular vein of horses and purified by centrifugation over discontinuous Percoll (Biochrom, Berlin, Germany) gradients as described (5). Cells were suspended at $0.5 \times 10^5$–$10^6$ cells/ml in Medium 199 (containing penicillin, streptomycin with 4.2 mM each of glutamine, and $NaHCO_3$), stored at room temperature, and used within 12 h of preparation. For fluorescence imaging combined with patch clamp capacitance measurements, ~30–50 μl of cell suspension was dispensed onto 25-mm glass coverslips held in a low wall Delrin chamber (ALA Scientific Instruments, Westbury, NY). External solution containing 140 mM NaCl, 10 mM HEPES, 5 mM KCl, 2 mM $CaCl_2$, 1 mM $MgCl_2$, 10 mM glucose, pH 7.2–7.3, ~300 mOsm containing 1 μM lysotracker green DND-26 (Molecular Probes, Eugene, OR) was added to the chamber to a final volume of about 1 ml. The cells were allowed to incubate in the dark for 45 min before the chamber was washed with external solution lacking the lysotracker dye.

*Electrophysiology*—Square wave whole-cell patch clamp methods were employed to measure passive electrical cell parameters (12, 13) during whole-cell stimulation with GTPγS.[1] Internal pipette solution contained 125 mM potassium glutamate, 10 mM NaCl, 7 mM $MgCl_2$, 4.5 mM $CaCl_2$, 5 EGTA-KOH, 1 mM ATP, 10 mM HEPES, pH 7.2, ~300 mOsm containing GTPγS concentrations as stated in the text. GTPγS stock solution was obtained from Roche Diagnostics.

Whole-cell current measurements were made with a HEKA EPC-9 patch clamp amplifier controlled by an Atari computer using a gain setting of 2 mV/pA, $t_r = 2$ μs and with the *C*-slow compensation turned off. A symmetrical square wave voltage stimulus with an amplitude of 20 or 32 mV (250 Hz) was generated by an analog/digital converter board (PCI-MIO-16XE-10; National Instruments, Austin, TX) and applied to the input of the EPC-9 on a holding potential of 0 mV. Currents were filtered using the 30-kHz 3-pole Bessel filter of the EPC-9 and continuously sampled at 100 kHz by the analog/digital converter board. Current transients were averaged and fit off-line using exponential curve fitting routines of IGOR Pro (Wavemetrics, Lake Oswego, OR). Cell membrane capacitance ($C_m$), conductance ($G_m$), and access resistance ($R_a$) circuit elements were obtained as described previously (12). A time delay introduced to the current transients by the amplifier current filter was corrected empirically by making small changes of the *C*-slow and $R_a$ controls of the EPC-9 with an open head stage until the effect of changes in the estimates of either circuit element on the other was at a minimum (12, 13). Single exponential fits were applied to all current

* This work was supported by National Institutes of Health Grant RO1NS38200 and the Nanobiotechnology Center (National Science Foundation Science and Technology Center supported by Agreement ECS-9876771). The costs of publication of this article were defrayed in part by the payment of page charges. This article must therefore be hereby marked "*advertisement*" in accordance with 18 U.S.C. Section 1734 solely to indicate this fact.

‡ To whom correspondence should be addressed: School of Applied and Engineering Physics, Cornell University, Ithaca, NY 14853. Tel.: 607-255-5264; Fax: 607-2557658; E-mail ml95@cornell.edu.

[1] The abbreviations used are: GTPγS, guanosine 5′-3-*O*-(thio)triphosphate; SNARE, soluble *N*-ethylmaleimide-sensitive factor attachment protein receptor; fF, femtofarad.

transients initially, and current transients that produced large fitting residuals were refit using a double exponential fitting routine. Equivalent circuit elements comprising the plasma membrane capacitance ($C_c$), fusing granule membrane capacitance ($C_g$), fusion pore conductance ($G_p$), cell membrane conductance ($G_m$), and pipette access resistance ($R_a$) were calculated as described previously (5).

*Fluorescence Imaging*—Wide-field epifluorescence imaging was performed on a Zeiss Axiovert 135 TV microscope using a 100 × 1.30 NA Fluar oil-immersion objective with a 1.6× Optovar setting. A cooled, intensified 12-bit CCD camera (Quantix 57; Photometrics, Tucson, AZ) was mounted to the top port of the microscope and connected to a PC computer running V++ software (Digital Optics, New Zealand). Images were acquired using 2 × 2 pixel binning, and the exposure times for image acquisition were between 40 and 100 ms. The image pixel size was 160 nm. Synchronization of the image acquisition and the electrophysiological measurements was effected by addition of the 5-V exposing output (scaled by 0.1 using a voltage divider) of the Quantix 57 camera to the whole-cell current at the analog/digital converter board for the initial 1 s of the measurements. Epi-illumination was obtained using a 75-watt xenon arc lamp that was strongly attenuated using a 0.1% transmission neutral density filter, and a 480/40 nm excitation filter, 505 nm LP dichroic, and a 535/50 nm emission filter (Omega Optical, Inc., and Chroma Technology, both of Brattleboro, VT). Under these imaging conditions, autofluorescence of eosinophil granules was not detectable, and photobleaching of lysotracker green was kept to a minimum. Experiments were performed at room temperature.

*Image Analysis*—Images were acquired and processed using V++ software and its built-in routines. Single frames ($n$) from acquired time-lapse sequences were extracted as signed 32-bit images. A subtraction procedure was implemented providing difference images according to the following scheme. For a sequence of $j$ number of images ($\text{image}_n \ldots \text{image}_{n+j-1}$) difference images ($\text{difference}_i = \textit{image}_i - \text{average}$, $i = n \ldots n + j - 1$) were generated by subtracting the average of 10 images preceding the first image in the following Sequence 1,

$$(\text{average} = \sum_{k=1}^{10} \text{image}_{n-k}/10)$$

SEQUENCE 1

The 32-bit difference images contained both negative and positive values. The difference images of the sequence ($n \ldots n + j - 1$) were scaled and converted to 8-bit gray scale images such that the minimum and maximum pixel values found in the difference image sequence were converted to values of 0 and 255, respectively. In some cases 10 sequential frames from the acquired time-lapse sequences were averaged into a single frame ($n$) and used to produce difference images. Fluorescence intensities of individual granules represent the mean pixel intensity from a 6 × 6 or 5 × 5 pixel region centered over a single granule. Whole-cell fluorescence intensity represents the mean pixel intensity from a rectangular region encompassing the cell.

*Cell Permeabilization and Electron Microscopy*—For electron microscopy cells were permeabilized at room temperature in internal solution containing 125 mM potassium glutamate, 10 mM NaCl, 7 mM $MgCl_2$, 3 mM EGTA, 1 mM ATP, 10 mM HEPES, 0.4 units/ml streptolysin-O, and 200 μM GTPγS, pH 7.2. After 0–12 min the cells were pelleted at 300 × *g,* and the supernatant was discarded. After a 15-min fixation in a solution containing 1% (w/v) glutaraldehyde, 5% (w/v) sucrose, 0.1 M cacodylate, pH 7.4, cells were washed in distilled water, treated with osmium tetroxide, dehydrated, washed with propylene oxide, and infiltrated with 50% propylene oxide/Epon. After another centrifugation, the supernatant was discarded, the pellet transferred to Epon, and polymerized at 56 °C for 48 h. Thin sections (100 nm) were transferred to Formvar-coated grids, stained with 3% (w/v) uranyl acetate in ethanol (6 min), washed 4 times with distilled water, and stained further with lead acetate. Electron microscopy was performed after thorough washing with water and dehydration.

## RESULTS

*Exocytosis of Single Granules*—Imaging of individual eosinophil granules stained with lysotracker green was facilitated in cells that had flattened on the glass coverslip bottom of the recording chamber (Fig. 1*A*). The cell was stimulated by intracellular application of 30 μM GTPγS via a patch pipette in the whole-cell configuration. Exocytosis of single granules manifests itself as a rapid disappearance of the fluorescent dye from discrete ~1.7-μm diameter fluorescent spots that is clearly evident from the difference images (Fig. 1*B*). The time course of fluorescent dye release from the two granules was obtained by plotting average fluorescence in the area covered by the respective granules (Fig. 1*C*). The membrane capacitance ($C_m$) measurement shows two discrete capacitance steps of ~50–60 fF (Fig. 1*D, dashed lines*) correlated in time (*vertical solid lines*) with the loss of fluorescent dye obtained by imaging. The capacitance increase of granule 1 occurs at 112.54 s (Fig. 1*D*). A faint fluorescence change is apparent in the subsequent frame, and fluorescence loss is complete within the next 2 frames (Fig. 1, *B* and *C*). Similarly, fusion pore opening of granule 2 indicated by the next capacitance step precedes release of the entrapped dye as observed previously (14) for exocytosis of giant granules from beige mouse mast cells. With a specific membrane capacitance of 9 fF/$\mu m^2$ (15), a spherical granule with a capacitance of 60 fF was estimated to be ~1.5 μm in diameter. We attributed the slightly larger size in the fluorescence image to the point spread function of the microscope and concluded that the loss of discrete fluorescent granule-size features represents exocytosis of single granules.

*Compound Exocytosis*—In the same cell at a later time, fluorescence was lost sequentially from 6 granules (Fig. 2*A*), but this loss of fluorescence was associated with one single but very large capacitance step of 480 fF (Fig. 2*B*), corresponding to the addition of 53 $\mu m^2$ of granule membrane to the plasma membrane. The capacitance step increase occurred over a period of less than 8 ms indicating a rapidly expanding fusion pore (data not shown). The 480 fF capacitance step occurred at 191.82 s of the recording time. The fluorescence loss from the first granule begins shortly after the capacitance step at 191.88 s (Fig. 2*C*). Subsequent loss of fluorescence from the other granules occurs over a period of 1 s (Fig. 2*C*) and is not associated with further capacitance changes (Fig. 2*B*). This result demonstrates that the 6 granules had already fused with one another preceding fusion of the compound granule with the plasma membrane. If 6 granules contributed to the 480-fF capacitance step, then an average granule membrane capacitance of 80 fF and granule diameter of ~1.7 μm was obtained consistent with the size of individual granules in these cells. Although in compound exocytosis release occurred through a single fusion pore, the individual granules do not release their contents simultaneously but sequentially.

The connectivity among granules and the plasma membrane during this compound granule fusion event may be inferred from the sequence of dye release from the compound granule (Fig. 2, *C* and *D*). By using the notation of Fig. 2, *C* and *D*, first granule 1 fuses with the plasma membrane and releases it contents, followed by granules 2 and 2′ that release their contents simultaneously. At the time when release from these granules started, the fluorescence decrease from granule 1 was slowed down, presumably reflecting release from granules 2 and 2′ through granule 1. Next granules 3 and 4 were released, associated with a slowing of the fluorescence decrease in granule 2, reflecting passage of the contents of granules 3 and 4 through granule 2. It should be noted that fluorescence loss from granule 2′ was very rapid because there was no passage of contents through granule 2′ from other granules. Finally, the content of granule 5 was released through the other granules, and the fluorescence decay of granule 1 goes to completion only when granule 5 had fully emptied.

Proof that all 6 granules were already fused at the time of release of granule 1 is provided by the single large membrane capacitance step that precedes the first release event (Fig. 2*B*). The granules had thus fused inside the cell without an obvious change in their morphology.

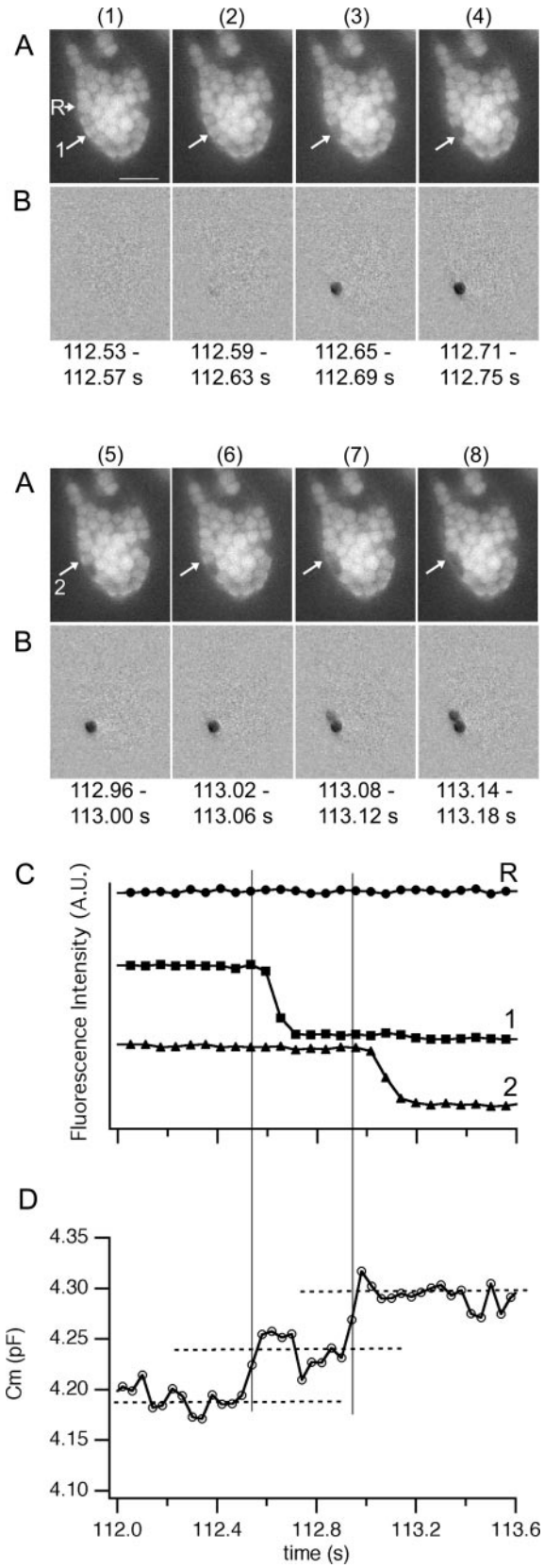


FIG. 1. **Exocytosis of individual granules labeled with lysotracker green in a horse eosinophil stimulated by intracellular application of 30 $\mu$M GTP$\gamma$S via a whole-cell patch pipette.** *A* (*top and bottom panels*), time-lapse fluorescence of images *1–8* obtained at 16 Hz indicates a sudden loss of fluorescence from two granules. The exposure period of each image is indicated *below* each frame. *Arrows* indicate the location of granule 1 in *frames 1–4* and the location of granule 2 in *frames 5–8*. *Scale bar* in *frame 1* is 5 $\mu$m. *B*, difference images of each image shown in *A* were produced by image subtraction as described under "Experimental Procedures." *Dark spots* indicate the loss of fluorescence intensity from individual granules. *C*, fluorescence intensity of granule 1, granule 2, and a reference granule (*R*) as indicated in *A* as a function of time. Granule 1 and granule 2 report a sudden loss of fluorescence, whereas the reference granule (located *above* granule 2) does not change in fluorescence intensity. *D*, cell membrane capacitance ($C_m$) measurements indicate two step-like increases of ~60 fF each at 112.54 and 112.94 s corresponding to the exocytosis of two individual granules.

*Stimulation of Granule-Granule Fusion Preceding Compound Exocytosis*—Are multigranular compounds present in resting cells or are they formed following stimulation of degranulation? Light microscopy cannot easily answer this question because granule-granule fusion is not associated with obvious morphological changes. However, intracellular granule-granule fusion could be observed following GTP$\gamma$S stimulation, taking advantage of variation in fluorescent staining among individual granules within the same cell following incubation with lysotracker green, similar to an observation made previously in mast cell granules stained with quinacrine (14). Differential loading of granules with the weak amine lysotracker green may occur due to differences in internal pH among the granules. In the cell shown in Fig. 3*A* (*left*), three granules appeared rather dim compared with the other granules (*arrows* denoted *1–3* in Fig. 3*A*). Fusion of a dim granule with a brighter granule should result in an increase of its fluorescence as their contents equilibrate. Conversely, fusion of a brighter granule with a dimmer granule should result in a respective decrease of its fluorescence. By 16.2 s, the fluorescence is much more homogeneous (Fig. 3*A*, *middle*), and the difference image (Fig. 3*A*, *right*) shows adjacent dark and bright spots suggesting transfer of fluorescent granule contents. Granules 1–3 show a fluorescence increase, whereas granules 1′–4′ show a fluorescence decrease. It should be noted that the fluorescence otherwise remains rather constant. No membrane capacitance changes occurred during this time. The fluorescence decrease in granules 1′–4′ is thus not due to exocytosis of these granules. The fluorescence changes are not due to granule movement (compare *left* and *middle panels* of Fig. 3*A*), which would produce white and dark edges in the difference image.

The fluorescence changes occurring in the individual granules were quantified by choosing 6 × 6 pixel regions centered over each granule providing the time course of mean pixel intensity. The fluorescence increase of granule 1 starts at 9.0 s (Fig. 3*B* (*1* and *1′*)). The fluorescence decrease in the adjacent granule 1′ has a similar time course suggesting that these signals reflect fusion between granule 1 and granule 1′. The onset of the fluorescence decrease of granule 2′ slightly precedes the fluorescence increase of granule 2, suggesting that they may not reflect fusion of these granules with each other but fusion with out-of-focus granules at slightly different times (Fig. 3*B* (*2* and *2′*)). Similarly, the fluorescence decrease of granule 3′ precedes the fluorescence increase of granule 3 (Fig. 3*B* (*3* and *3′*)). The fluorescence decrease of granule 4′ starts before all other changes and has a slow time course (Fig. 3*B* (*4′*)). Additional fusion events between granules with similar fluorescence levels or fusion of granules in out-of-focus image planes may have occurred but would not be detectable. Because none of the fluorescence changes are associated with capacitance steps, they therefore reflect intracellular granule-granule fusion events.

In the same cell at a later time (25.44 s), a fusion pore formed with a conductance ($G_p$) of 3.5 nS, between a very large multigranular compound with a capacitance ($C_g$) of 2.4 pF and the plasma membrane (Fig. 3, *C* and *D*). The compound connected to the plasma membrane by a narrow fusion pore has a slower

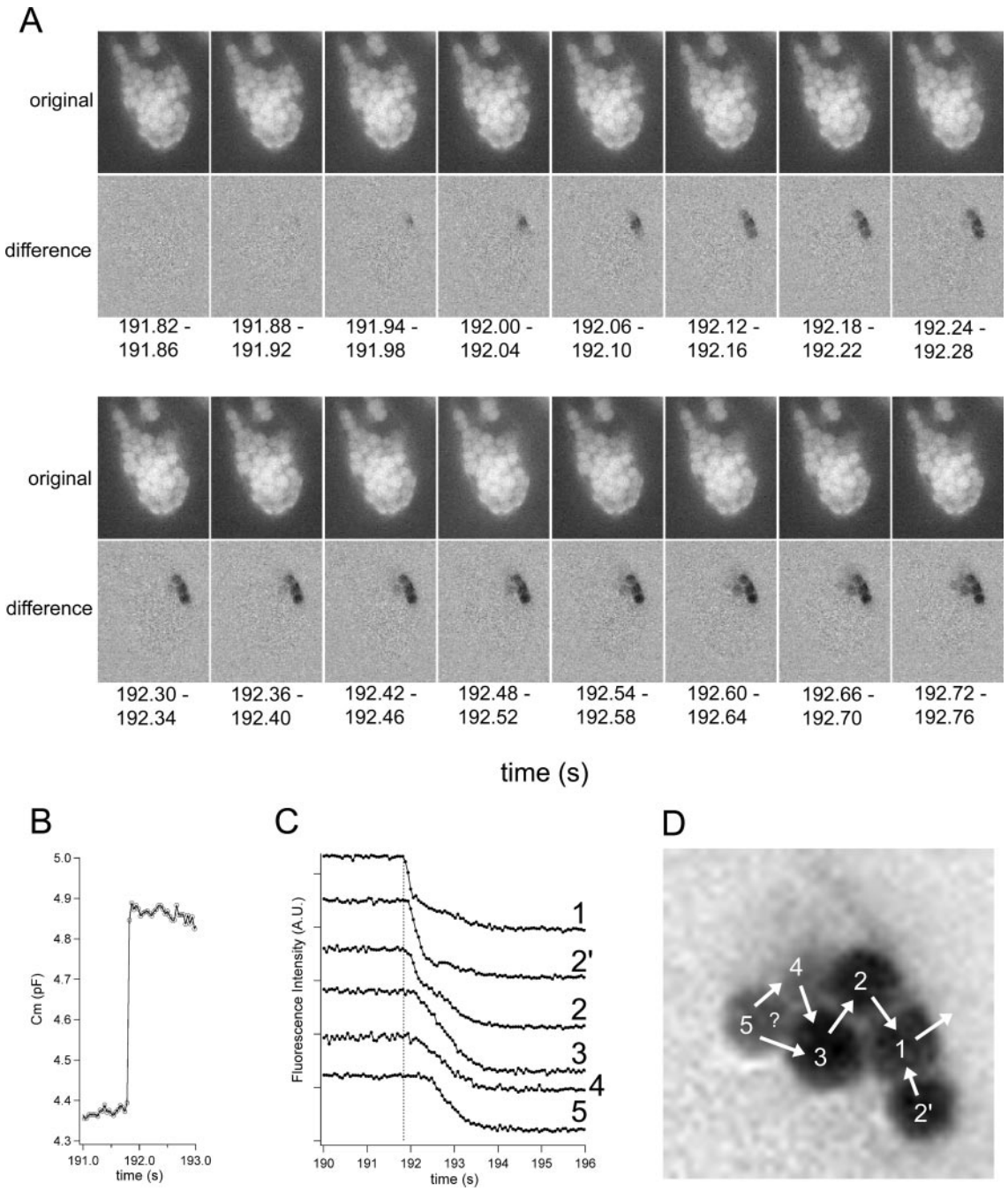


FIG. 2. **A compound fusion event observed in the same cell shown in Fig. 1.** *A*, time-lapse fluorescence images indicating a progressive loss of dye from 6 fluorescent granules. The exposure period of each image is indicated. Difference images shown *below* the original images were obtained as described under "Experimental Procedures." *B*, cell membrane capacitance ($C_m$) recording shows a large single step increase of 480 fF at 191.8 s. *C*, fluorescence intensities of the 6 exocytosed granules indicated in *A* as a function of time. *D*, difference images obtained by subtraction of an average of images taken before (191.16–191.70 s) and after (193.56–194.10 s) compound exocytosis show loss of fluorescent dye from 6 adjoining granules. *Numbers* and *arrows* represent the sequence and direction of dye loss derived from the traces shown in *C*. In the difference images *dark areas* indicate a loss of fluorescence intensity.

capacitive charging time constant than the plasma membrane. In response to square pulse voltage steps, a capacitive current transient with a slow charging time constant appears in parallel with the faster capacitive transient of the plasma membrane (5). These components can thus be separated by fitting the current transients with the sum of two exponentials providing the capacitance of the plasma membrane ($C_c$), the compound granule capacitance ($C_g$), and the fusion pore conductance ($G_p$), in addition to cell membrane conductance ($G_m$) and access resistance ($R_a$) as illustrated in Fig. 3*C*.

The exocytosed compound thus forms a degranulation sac with $C_g$ = 2.4 pF. This step size corresponds to a compound consisting of about 35 granules. $C_g$ then increases to a final value of 3.5 pF, presumably reflecting fusion of another ~15 granules with the degranulation sac after the fusion pore has formed. At 32.4 s, $G_p$ increases to a very large value. The charging time constant of the degranulation sac becomes very fast, and the capacitance of the degranulation sac and the capacitance of the plasma membrane cannot be distinguished anymore. At this time the $C_g$ becomes part of the plasma membrane ($C_c$) which accordingly increases by ~3.5 pF (Fig. 3*D*).

As observed previously (14) for the giant granules of beige mouse mast cells, release of fluorescent dye (Fig. 3*D*, *fluores-*

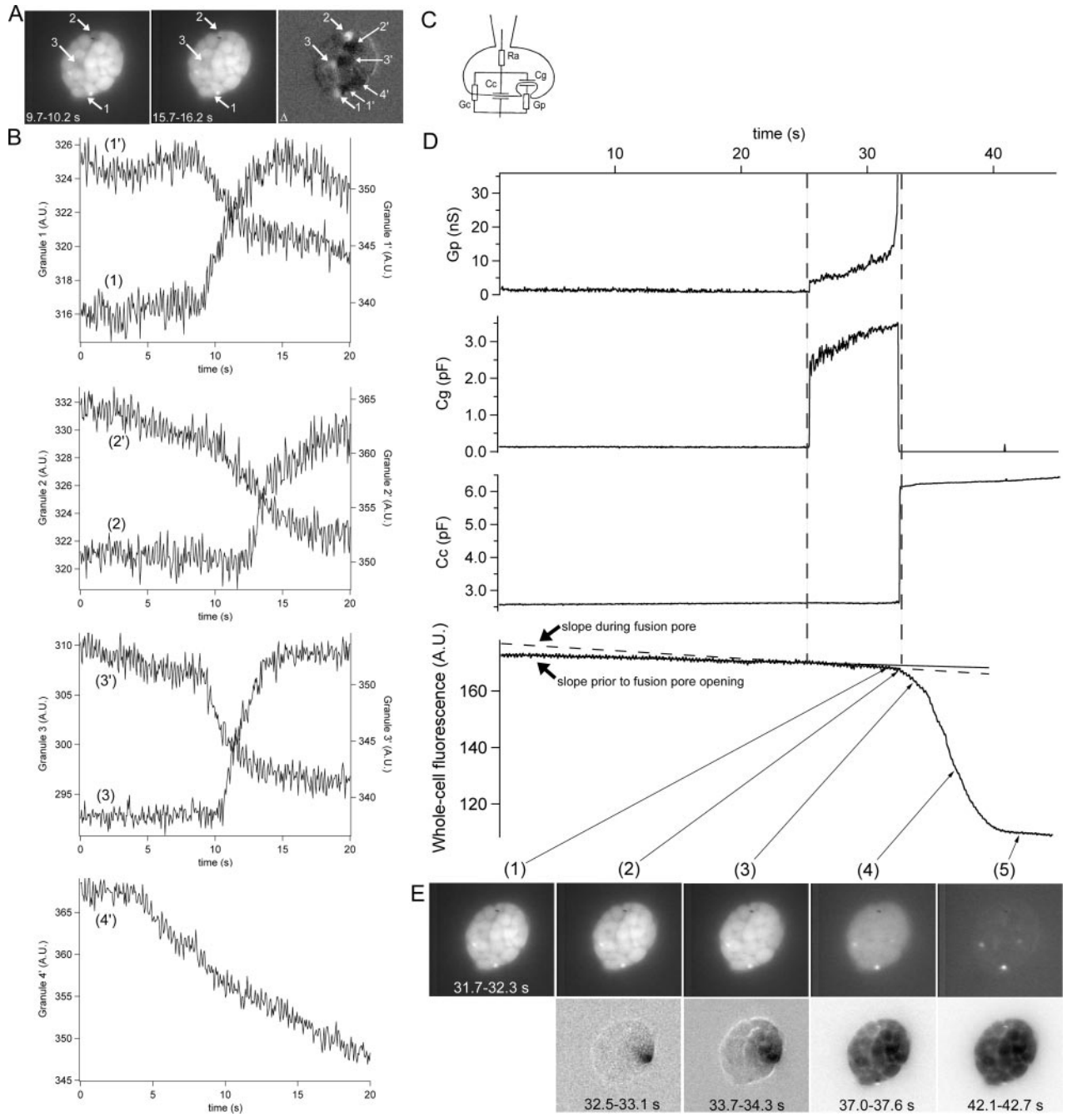


FIG. 3. **Intracellular granule-granule fusion precedes compound exocytosis.** Pipette GTPγS concentration was 150 μM. *A*, images taken during whole-cell stimulation of a horse eosinophil labeled with lysotracker green. Images (*left* and *middle*) are averages of single frames spanning the exposure period indicated. The difference between these images, Δ (*right*), shows bright granules (*labeled 1–3*) indicating an increase in fluorescence and dark granules (labeled *1′–4′*) indicating a decrease in fluorescence. *B*, time course of fluorescence intensity for the labeled granules. *C*, whole-cell equivalent circuit indicating pipette access resistance $R_a$, cell membrane conductance $C_c$, cell membrane capacitance $C_c$, and a degranulation sac of capacitance $C_g$ connected to the extracellular space via a fusion pore with conductance $G_p$. *D*, time course of $G_p$ (*top trace*), $C_g$ (*2nd trace*), $C_c$ (*3rd trace*), and whole-cell fluorescence (*bottom trace*). The whole-cell fluorescence time course was fit by linear regression for the time preceding fusion pore opening (*continuous line*) and during the existence of a narrow fusion pore indicated between *dashed vertical lines. E*, original (*top*) and difference (*bottom*) images for the times indicated by the *arrows* to the fluorescence trace. The difference images had to be scaled individually to clearly show the fluorescence gradients for each difference image.

*cence trace*) is hardly detectable until the fusion pore conductance becomes very large at 32.4 s (Fig. 3*D*, $G_p$ *trace*). However, slow release of secretory products does occur through fusion pores with small conductance (15, 16). Before the fusion pore formed, the whole-cell fluorescence (Fig. 3*D*) decreased slowly and linearly (*straight solid line*), presumably due to photobleaching of lysotracker green. After fusion pore formation, although the fusion pore is small (*between vertical lines*), the linear regression yields a significant increase in slope (*dashed line*) of the fluorescence decrease indicative of slow release through the narrow fusion pore. It should be noted that very little morphological changes occur before the fusion pore conductance increases to a large value. The increase of fusion pore conductance is followed by a rapid loss of fluorescent dye.

The large fusion pore conductance could reflect either a single large pore or the formation of a large number of smaller pores. If one single large pore is formed, then release should occur at one focal site. Indeed, as shown in difference images

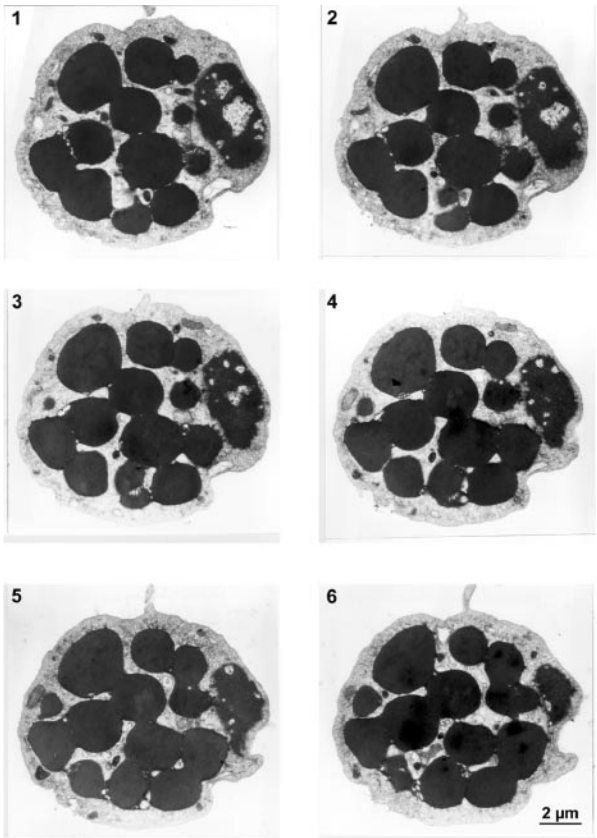


FIG. 4. **Electron microscopy of a multigranular compound.** Serial 100-nm sections from a single streptolysin-O permeabilized eosinophil stimulated with 200 μM GTPγS. *Numbers 1–6* indicate the section sequence. The secretory granules are connected together forming a compound containing virtually all granules. Note that the interconnected granules retain their morphology and dense contents.

presented in Fig. 3*E*, loss of the dye is first detectable at a focal spot at the plasma membrane. Originating from this point the fluorescence decrease expands indicating focal release through a single pore.

A few seconds later, the cell is nearly devoid of visible granules and fluorescent dye (Fig. 3*E*, *frame 5*) with the exception of a few small bright spots, indicating secretion of the contents from the entire intracellular pool of ~50 granules through a single fusion pore. These results demonstrate directly that compound exocytosis in eosinophils is preceded by intracellular granule-granule fusion and that a narrow fusion pore forms between the compound granule and the plasma membrane which allows for focal release upon fusion pore dilation.

*Electron Microscopy of Compound Exocytosis*—Compound exocytosis becomes more prevalent when GTPγS is introduced into the cell at 100–200 μM concentration (5). To capture compound formation by electron microscopy before exocytosis occurs, cells were permeabilized with streptolysin-O and stimulated with 200 μM GTPγS. At this concentration all granules may fuse inside the cell leading to compound exocytosis with a single capacitance step of ~3 pF (17). Fig. 4 shows serial sections from a cell that was fixed several minutes after addition of streptolysin-O and GTPγS. When the different planes are considered, it becomes apparent that all granules are interconnected. However, no exocytosis has occurred yet since all granules have retained their dense core. Cells that were fixed immediately after stimulation did not show such features. In the permeabilized cells granule shape was somewhat distorted, but cytosolic space is clearly visible between adjacent granules (Fig. 5*A*). At later stages, when exocytosis has occurred, the

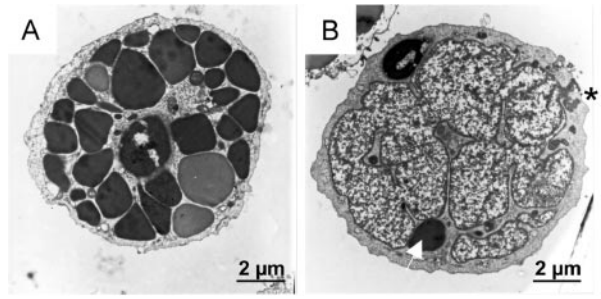


FIG. 5. *A*, a cell fixed shortly after stimulation shows no granule-granule fusion. *B*, a later stage of degranulation. The cell contains a large degranulation sac connected to the outside via an expanded fusion pore (*asterisk*). One granule shows no sign of exocytosis (*arrow*).

granular contents within the degranulation vacuole appear less dense (Fig. 5*B*) whereas at least one unfused granule (*arrow*) has retained its dense core.

*Cumulative Fusion and Formation of a Degranulation Sac*—An alternative mode of exocytosis called sequential or cumulative exocytosis has been proposed to produce a degranulation sac and focal release during eosinophil degranulation (5, 9). In this mode granules fuse sequentially to a granule already connected to the plasma membrane by a narrow fusion pore. Fluorescence microscopy of cells stimulated with low (5 μM) GTPγS concentration directly visualizes this mode of exocytosis (Fig. 6). The capacitance measurement (Fig. 6*A*) reveals an increase in a number of steps, many of which have the size expected for individual granules and compounds that consist of a few granules. As in the analysis presented in Fig. 3, $C_c + C_g$ was determined from double exponential fits. When $C_g$ and $C_c$ are plotted separately (Fig. 6*A* $C_g$, $C_c$), most of the capacitance increase occurs in $C_g$, suggesting formation of a growing degranulation sac. During the stepwise increase of $C_g$, the fusion pore of the degranulation sac shows an uncorrelated fluctuating increase in fusion pore conductance ($G_p$).

Fig. 6*B* shows the associated cellular morphological changes. Initially, a few exocytotic events occur near the left edge of the cell, accompanied by the first capacitance steps. Then an exocytotic event at the right edge is followed by cumulative fusion such that a degranulation sac of increasing size is formed. The morphological disappearance of individual granules indicates contact with extracellular space via a fusion pore. Further granules fuse and blend into the growing degranulation sac. The morphological appearance of the degranulation sac is correlated with the appearance of a growing capacitance $C_g$, connected to the extracellular space via a fusion pore with rather low conductance. Accordingly, the fluorescence from individual granules equilibrates, but the overall loss of fluorescence is very slow due to the limiting size of the fusion pore.

The initial development of a degranulation sac is revealed in detail by correlating capacitance changes with the loss of fluorescence intensity from individual granules. Fig. 6*C* shows the change of fluorescence intensity of the granules labeled *1–6* in Fig. 6*D*. The change in fluorescence for each granule is correlated with distinct steps in the membrane capacitance traces as indicated by the *vertical arrows* in Fig. 6, *A* and *C*. By using the notation of Fig. 6, *C* and *D*, granule 1 first fuses with the plasma membrane. The rapid fluorescence decrease from this peripheral granule immediately follows a capacitance step appearing in the $C_g$ trace. The next capacitance step is associated with a fluorescence loss in granule 2 and a fluorescence increase in granule 1 demonstrating directly that this capacitance step reflects fusion of granule 2 with granule 1 and not fusion of granule 2 with the plasma membrane. Accordingly, this fusion event appears clearly in $C_g$, reflecting a cumulative

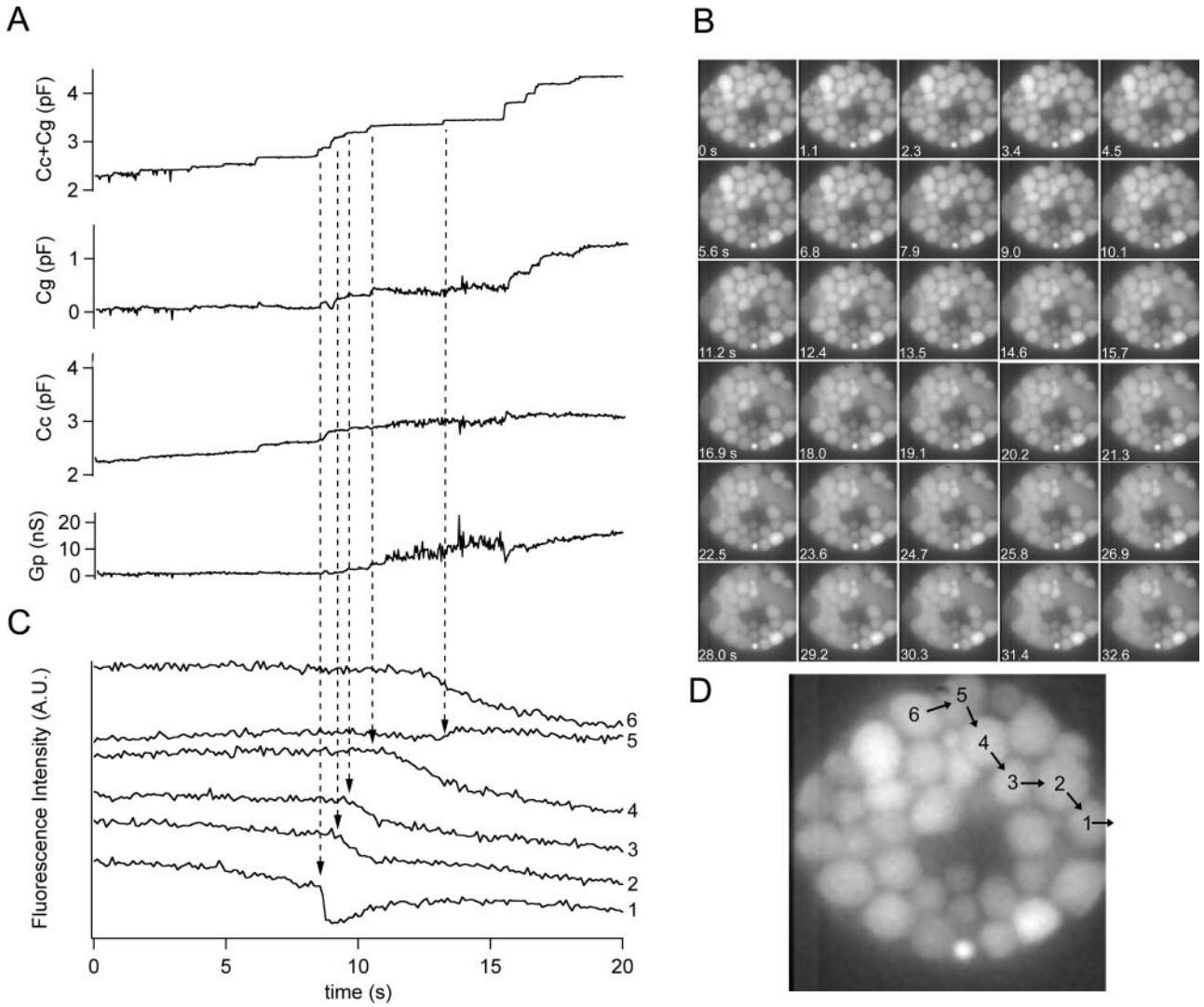


FIG. 6. **Cumulative exocytosis in a horse eosinophil stimulated with 5 $\mu$M GTP$\gamma$S.** *A*, time course of $C_c + C_g$, $C_g$, $C_c$, and $G_p$ from analysis using the equivalent circuit of Fig. 3*C*. *B*, time-lapse fluorescence images of the cell. Granules were labeled with lysotracker green. Averaged images shown were obtained by averaging 10 sequential 100.06-ms exposure images spanning a period of 1.1222 s. The rounded exposure start time is indicated on each frame. *C*, time course of fluorescence intensity for the labeled granules. *Arrows* indicate correlation of fluorescence intensity changes and capacitance steps that could be assigned to individual granules. *D*, enlargement of an image from *B* at $t = 0$ s. *Numbers* and *arrows* represent the sequence of cumulative fusion of 6 granules derived from the traces shown in *C*.

increase in the area of the degranulation sac.

Subsequently, granules 3 and 4 also fuse in a sequential manner with granule 2 as illustrated in Fig. 6*D* and contribute capacitance steps that increase the capacitance of the growing degranulation sac. The relatively dim granule 5 then undergoes a sudden increase in fluorescence associated with the next capacitance step indicating that it also fuses with the degranulation sac. The onset in the fluorescence decrease of granule 6 slightly precedes this fusion event suggesting that it likely fuses with granule 5 before fusion of granule 5 with the degranulation sac. The cumulative fusion of these granules is also evident morphologically on the right-hand side of the cell in the associated fluorescence images acquired between 7.9 and 15.7 s.

Examination of the remaining recording shows that the capacitance of the degranulation sac, $C_g$, continues to grow in size by ~0.91 pF with the cumulative addition of ~14 granules (average granule capacitance = 65 fF). No further changes in the capacitance measurement occur after 20 s (data not shown). Indeed, another 14 granules clearly visible in the 15.7 s image lose their structural integrity, blending onto the degranulation sac (Fig. 6*B*). These changes are very slow and extend beyond the last exocytotic event that occurred at about 18 s (compare image *20.2* and *32.6 s* Fig. 6*B*). During this second phase of capacitance increase to $C_g$ (between 14 and 20 s), an unambiguous assignment of fluorescence changes in individual granules with certain capacitance steps is troublesome due to the slow rate of release of dye from fused granules within the degranulation sac. The cumulative fusion events produced a degranulation sac with a large volume, while the fusion pore conductance was still only ~10 nS (Fig. 6*A*, $G_p$). The fluorescence between all granules in the sac thus equilibrated, and further lysotracker dye loss was very slow as seen in the traces of Fig. 6*C* and in the images of Fig. 6*B*.

## DISCUSSION

The main physiological function of eosinophils is thought to be in defense against parasitic infection. These cells can kill various parasites, in particular at the larval stage (18). The release of cytotoxic proteins from eosinophil granules onto the parasite surface plays an important role in parasite killing. On the other hand, eosinophil degranulation can also lead to tissue damage in some types of allergic asthma (19). For the physiological function of eosinophils it is thus essential that release of

granule contents is focused onto the target and that diffusion of cytotoxic proteins to host tissue cells is prevented.

By using combined patch clamp capacitance measurements and fluorescence imaging, we demonstrate directly that focal release from eosinophils occurs by two mechanisms. In compound exocytosis, intracellular granule-granule fusion can lead to formation of a large multigranular compound that releases its contents through a single fusion pore. Compound exocytosis has been demonstrated for lamellar body exocytosis in alveolar type II cells by using a similar approach combining capacitance measurements and FM1-43 fluorescence imaging (20). Growing fluorescent spots indicating cumulative fusion were also observed in stimulated pituitary lactotrophs (21).

In eosinophils intracellular granule-granule fusion is not associated with morphological changes visible in the light microscope but is clearly evident from fluorescent content transfer and in electron microscopy. Changes in granule morphology require solubilization of granule cores. Dissolution of acidic chromaffin granule contents occurs under alkaline conditions (22). Eosinophil granules are also acidic organelles (23), and therefore it is a possibility that the consecutive solubilization of granule contents during compound exocytosis occurs due to consecutive granule core alkalization. In pituitary lactotrophs, dissolution of granule cores was markedly enhanced by treatments that reduced cytosolic cAMP concentration suggesting a mechanism regulating the susceptibility of granules to undergo solubilization following exocytosis and exposure to neutral pH (24).

Previous electrophysiological studies suggested that in eosinophils focal release is also achieved by formation of a degranulation sac from cumulative granule fusion events (5). In cumulative fusion a granule performs exocytotic fusion with the plasma membrane followed by daisy chain fusion of additional granules. Fluorescence imaging (Fig. 6) directly visualizes the formation of a growing degranulation sac, and the multiple capacitance steps associated with this process show that these previously are sequential fusion events. Such cumulative fusion sequences have been reported for exocytosis of zymogen granules, studied in intact pancreatic acini by multiphoton fluorescence microscopy (25). Zymogen granules fused with the plasma membrane, maintained their Ω shape and served as targets for sequential fusion of granules located within deeper layers of the cell, such that transport of granules to the plasma membrane was not required (25).

In eosinophils a cumulative fusion mechanism ensures focal release. It was shown in mast cells that local stimulation induces local degranulation (26). Similarly, stimulation of eosinophils upon contact with a parasite may initiate exocytosis at the site of contact that would then be followed by cumulative fusion leading to focal release. In the experiments described here, cells were stimulated by intracellular application of GTPγS. Even with this delocalized stimulus focal release occurs. This mechanism requires that the rate at which cytoplasmic granules fuse with the membrane of previously exocytosed granules is much higher than the rate at which they fuse with the plasma membrane. The fusion of eosinophil granules with the plasma membrane is thus a rare event, which ensures that focal release preferentially occurs through a single fusion pore.

The molecular mechanisms controlling granule-granule fusion, compound, and cumulative exocytosis in eosinophils are not known. In lactotrophs, the incidence of compound exocytosis was found to increase upon incubation with phorbol ester (21) pointing toward a controlling role of protein kinase C. It has been suggested that cumulative exocytosis of granules to previously fused granules (in pancreatic acinar cells) is mediated by the transfer of a plasma membrane protein, possibly a SNARE protein to the granule membrane because there was no evidence for intracellular granule-granule fusion (25). However, as shown here, in eosinophils granule-granule fusion does occur indicating that the required SNARE proteins must be present on the granule membrane. In mast cells, compound exocytosis is dependent on the translocation of SNAP-23 (synaptosome-associated protein) from the plasma membrane to granule membrane (27), whereas in *Drosophila*, SNAP-24, which is resident on glue protein-containing granules in salivary gland cells, has also been implicated in regulating compound exocytosis (28).

SNARE proteins are expressed in eosinophils (29–31), but their roles in compound and cumulative exocytosis remain unexplored. In eosinophils, high GTPγS concentration increases the incidence of compound exocytosis (5) implicating a GTP-binding protein in the control of granule-granule fusion. The differential regulation of granule-granule fusion, cumulative fusion, and granule-plasma membrane fusion by calcium and GTP-binding proteins is investigated in the accompanying paper (32).

*Acknowledgments*—We thank Carol Collyer (Director of Equine Services at the Equine Research Park, Cornell University) and Lori Kwan and Joan Lenz for excellent technical assistance in obtaining blood and isolating horse eosinophils.

REFERENCES

1. Butterworth, A. E. (1977) *Curr. Top Microbiol. Immunol.* **77,** 127–168
2. Lacy, P., and Moqbel, R. (2001) *Curr. Opin. Allergy Clin. Immunol.* **1,** 79–84
3. Henderson, W. R., Chi, E. Y., Jörg, A., and Klebanoff, S. J. (1983) *Am. J. Pathol.* **111,** 341–349
4. Nüsse, O., Lindau, M., Cromwell, O., Kay, A. B., and Gomperts, B. D. (1990) *J. Exp. Med.* **171,** 775–786
5. Scepek, S., and Lindau, M. (1993) *EMBO J.* **12,** 1811–1817
6. Tai, P.-C., and Spry, C. J. F. (1981) *Br. J. Hematol.* **49,** 219–226
7. McLaren, D. J., Mackenzie, C. D., and Ramalho-Pinto, J. F. (1977) *Clin. Exp. Immunol.* **30,** 105–118
8. Glauert, A. M., Butterworth, A. E., Sturrock, R. F., and Houba, V. (1978) *J. Cell Sci.* **34,** 173–192
9. Dvorak, A. M., Galli, S. J., Morgan, E., Galli, A. S., Hammond, M. E., and Dvorak, H. F. (1981) *Lab. Investig.* **44,** 174–191
10. Scepek, S., Moqbel, R., and Lindau, M. (1994) *Parasitol. Today* **10,** 276–278
11. Henderson, W. R., and Chi, E. Y. (1985) *J. Cell Sci.* **73,** 33–48
12. Lindau, M., and Neher, E. (1988) *Pfluegers Arch. Eur. J. Physiol.* **411,** 137–146
13. Thompson, R. E., Lindau, M., and Webb, W. W. (2001) *Biophys. J.* **81,** 937–948
14. Breckenridge, L. J., and Almers, W. (1987) *Proc. Natl. Acad. Sci. U. S. A.* **84,** 1945–1949
15. Albillos, A., Dernick, G., Horstmann, H., Almers, W., Alvarez de Toledo, G., and Lindau, M. (1997) *Nature* **389,** 509–512
16. Alvarez de Toledo, G., Fernández-Chacón, R., and Fernandez, J. M. (1993) *Nature* **363,** 554–558
17. Lindau, M., Hartmann, J., and Scepek, S. (1994) *Ann. N. Y. Acad. Sci.* **710,** 232–247
18. Meeusen, E. N., and Balic, A. (2000) *Parasitol. Today* **16,** 95–101
19. Walsh, G. M. (1999) *Crit. Rev. Clin. Lab. Sci.* **36,** 453–496
20. Mair, N., Haller, T., and Dietl, P. (1999) *Am. J. Physiol.* **276,** L376–L382
21. Cochilla, A. J., Angelson, J. K., and Betz, W. J. (2000) *J. Cell Biol.* **150,** 839–848
22. Yoo, S. H. (1996) *J. Biol. Chem.* **271,** 1558–1565
23. Kurashima, K., Numata, M., Yachie, A., Sai, Y., Ishizaka, N., Fujimura, M., Matsuda, T., and Ohkuma, S. (1996) *Lab. Investig.* **75,** 689–698
24. Angleson, J. K., Cochilla, A. J., Kilic, G., Nussinovitch, I., and Betz, W. J. (1999) *Nat. Neurosci.* **2,** 440–446
25. Nemoto, T., Kimura, R., Ito, K., Tachikawa, A., Miyashita, Y., Iino, M., and Kasai, H. (2001) *Nat. Cell Biol.* **3,** 253–258
26. Lawson, D., Fewtrell, C., and Raff, M. (1978) *J. Cell Biol.* **79,** 394–400
27. Guo, Z., Turner, C., and Castle, D. (1998) *Cell* **94,** 537–548
28. Niemeyer, B. A., and Schwarz, T. L. (2000) *J. Cell Sci.* **113,** 4055–4064
29. Hoffmann, H. J., Bjerke, T., Karawajczyk, M., Dahl, R., Knepper, M. A., and Nielsen, S. (2001) *Biochem. Biophys. Res. Commun.* **282,** 194–199
30. Lacy, P., Logan, M. R., Bablitz, B., and Moqbel, R. (2001) *J. Allergy Clin. Immunol.* **107,** 671–678
31. Logan, M. R., Lacy, P., Bablitz, B., and Moqbel, R. (2002) *J. Allergy Clin. Immunol.* **109,** 299–306
32. Hartmann, J., Scepek, S., Hafez, I., and Lindau, M. (2003) *J. Biol. Chem.* **278,** 44928–44933


Membrane Transport, Structure, Function, and Biogenesis:

# Compound Exocytosis and Cumulative Fusion in Eosinophils

Ismail Hafez, Andreas Stolpe and Manfred Lindau

*J. Biol. Chem. 2003, 278:44921-44928.*
*doi: 10.1074/jbc.M306013200 originally published online August 15, 2003*